Supporting material for:

Experimental and Theoretical Investigation into Visible–light–promoted Selective Hydrogenation of Crotonaldehyde to Crotonyl Alcohol using Au–Co,Ni Alloy Nanoparticles Supported Layered Double Hydroxides

Guanhua Zhang[a], Xiaofeng Zhang[a], Yue Meng[b], Xiaobo Zhou[c], Guoxiang Pan[b], Zheming Ni[a]*, Shengjie Xia[a]*

[a] *Department of Chemistry, College of Chemical Engineering, Zhejiang University of Technology, Hangzhou 310032, P R China*

[b] *Department of Materials Engineering, Huzhou University, Huzhou 313000, P R China*

[c] *Entegris, Inc., 129 Concord Road, Billerica, MA 01821, USA*

* Corresponding author.

E–mail: xiasj@zjut.edu.cn (S.J. Xia); jchx@zjut.edu.cn (Z.M. Ni)

Telephone number: 086–0571–88320373

1. Experimental supplements

1.1 Materials

Chloroauric acid ($HAuCl_4$) and sodium borohydride ($NaBH_4$) were guarantee reagent (GR) and purchased from Aladdin Chemistry Co. Ltd. Cobalt nitrate ($Co(NO_3)_2 \cdot 6H_2O$), nickel nitrate ($Ni(NO_3)_2 \cdot 6H_2O$), aluminum nitrate ($Al(NO_3)_3 \cdot 9H_2O$), zinc nitrate ($Zn(NO_3)_2 \cdot 6H_2O$) and sodium carbonate ($Na(CO_3)_2$) were analytical reagent (AR) and all purchased from Guoyao Fine Chemical Co. Ltd. In addition, ultrapure water was used in all synthetic process.

1.2 Characterizations

Powder X–ray diffraction (XRD) was recorded on a Rigaku UltimaIV powder diffractometer with the testing of Cu Kα radiation (λ = 1.54 Å) at 40 kV and 178 mA and scanning rate of 5 °/min in the range of 5–70 °. C, H and N elemental microanalyses were obtained on a ThermoFisher Italia S.P.A elemental analyzer; the analysis of Au, Co, Ni, Zn and Al elements was conducted using inductively coupled plasma atomic emission spectrometry (ICP–AES) on a IRIS Intrepid II XSP instrument. Solid state UV–vis diffuse reflectance spectra was recorded at room temperature in the air by means of a Shimadzu UV–2600 spectrometer equipped with an integrating sphere attachment. $BaSO_4$ was used as background. The products of crotonaldehyde hydrogenation and their concentrations were tested by Shimadzu GC–2014C. The TEM with EDX was recorded on a Hitachi HT–7700 to examine the morphologies, lattice fringes and crystal boundaries of the samples.

1.3 Theoretical calculation

1.3.1 Calculation methods and parameters

DFT calculation is based on the combination of general gradient analysis and Perdew–Wang–91 (GGA–PW91), the calculation work was done using the Dmol[3]

package in Materials Studio 8.0. We used frozen–core approximation to simulate the inner layer electrons, replace them with ECP. Valence electron wave function was expanded by double numeric with polarization (DNP). The *k* grid of Brillouinzone integration was set at 3×3×1, grid parameter was chosen as Medium, Methfessel–Paxton smearing was 13.1 kJ/mol. We did not turn off electron spinning as the spin polarization has little influence onto the adsorption model. The structure optimization was based on energy difference, atomic displacement and the interaction convergence. The numbers for each convergence standard are as follows: 4.8×10^{-2} kJ/mol, 5.0×10^{-4} nm and 9.7 kJ/(mol·nm). Above mentioned optimization was used to all the reactants and reaction products for the elementary reactions; the optimized structure was used as the initial and final states and then was further screened by transition state (TS) search, using the combination of linear synchronous transformation (LST) and quadrate synergistic transformation (QST) methods. The optimized structure was confirmed to have only one imaginary frequency.

1.3.2 Periodical models

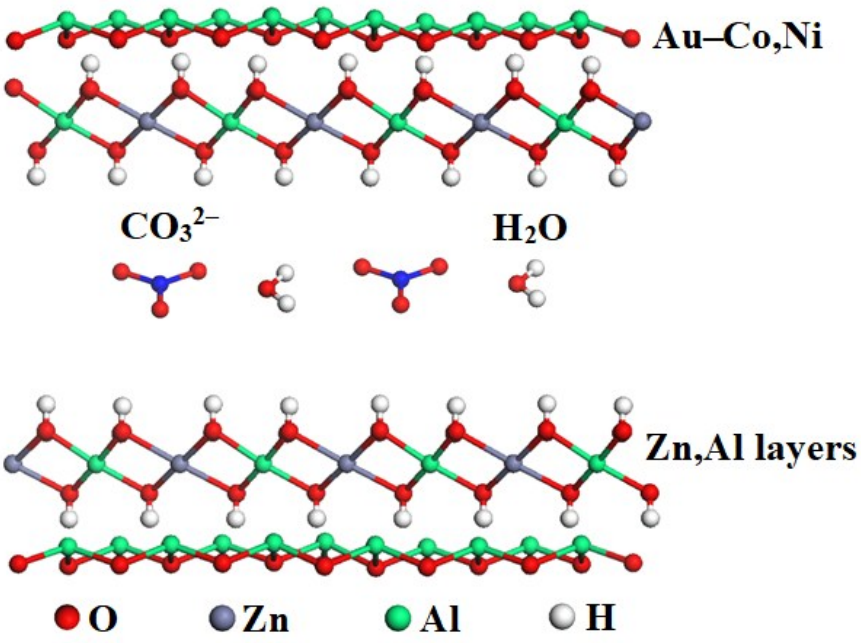

Figure S1(A) Structural model of Au–Co,Ni/LDHs.

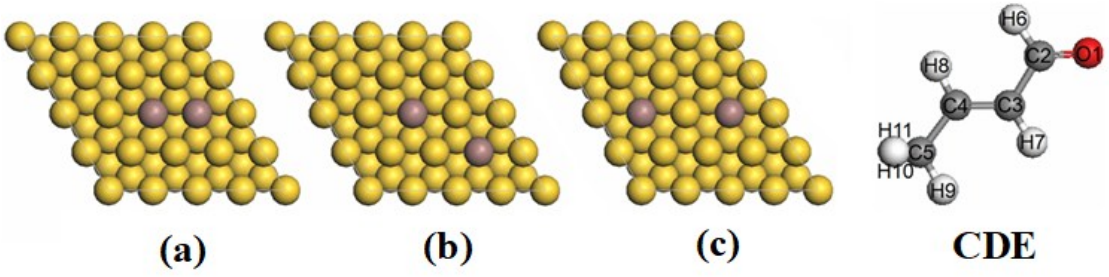

Figure S1(B) Different models of (111) facet of Au crystal partial substituted by Co or Ni (Au–Co,Ni) and the structure of CDE.

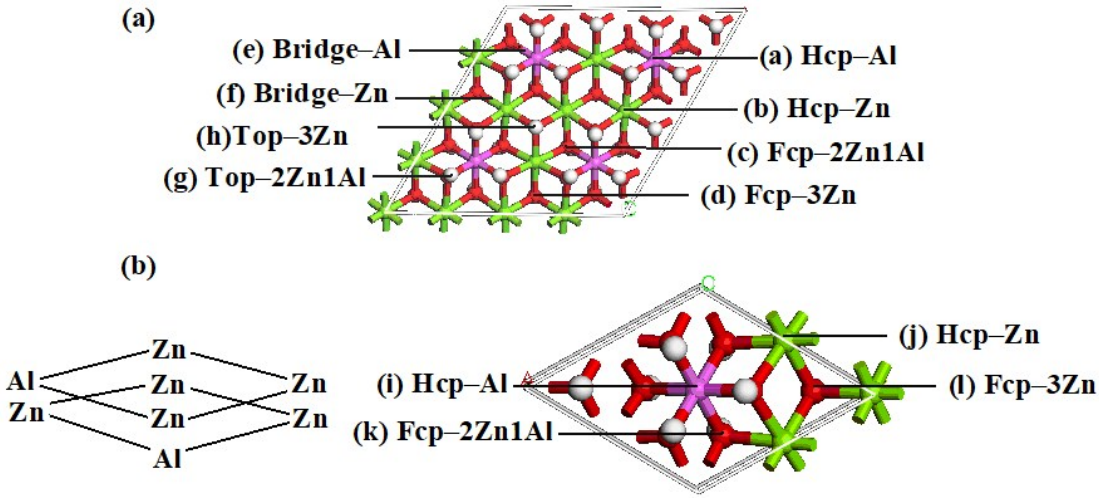

Figure S1(C) Periodical double layer models of ZnAl–LDHs: (a) Al symmetry 2x2; (b) Al dissymmetry 1x1.

Au–Co,Ni/ZnAl–LDHs periodical double layer model was built based on 2H packing and also based on putting (111) facet of Au crystal partial substituted by Co or Ni on two layers of ZnAl–LDH surfaces. **Fig. S1(A)** shows the structural model for Au–Co,Ni/ZnAl–LDHs.

We chose the low coverage (1/16)*p*(4×4) periodic model to simulate Au(111), the vacuum layer is set at 1.20 nm to avoid mirror effect between the layers. Based on this model, we replaced two Au atoms at the surface of Au(111) to construct the model of Au–Co,Ni/LDHs surface [S1,S2]. We further made 3 different models based on the

distance of the position of modified element atom, which are marked as a, b and c in **Fig. S1(B)**. in addition, we also used frozen core for the bottom layers of atoms and top 2 layers are free mobile, surface relaxation was also taken into account during the calculation. **Fig. S1(B)** also shows the CDE structure.

The anion interaction site in the LDHs layer was discussed by using CO_3–LDHs as the model; water molecule was not introduced into the layer model in order to simplify the calculation. The layered anions could interact with the LDHs layer with multiple possible sites. In the case of symmetrical layered Al^{3+}, the layered anion could exist at 8 different sites on the LDHs layer, as **Fig. S1(C–a)** tells. In addition, when Al^{3+} was intercostal positioned in the layer (Al^{3+} is exchanged with the neighboring Zn^{2+}), we only calculated the 4 configurations when CO_3 anion was at Hcp and Fcp sites, as displayed in **Fig. S1(C–b)**.

[S1] Zhao J., Ni J., Xu J.H., Xu J.T., Cen J., Li X.N. Ir promotion of TiO_2 supported Au catalysts for selective hydrogenation of cinnamaldehyde. *Catalysis Communications*, **2014**, 54: 72–76.

[S2] Mohr C., Hofmeister H., Radnik J., Claus P. Identification of active sites in gold–catalyzed hydroge nation of acrolein. *Journal of the American Chemical Society*, **2003**, 125(7): 1905–1911.

2. Results and discussion supplements

2.1 Characterization supplements of samples

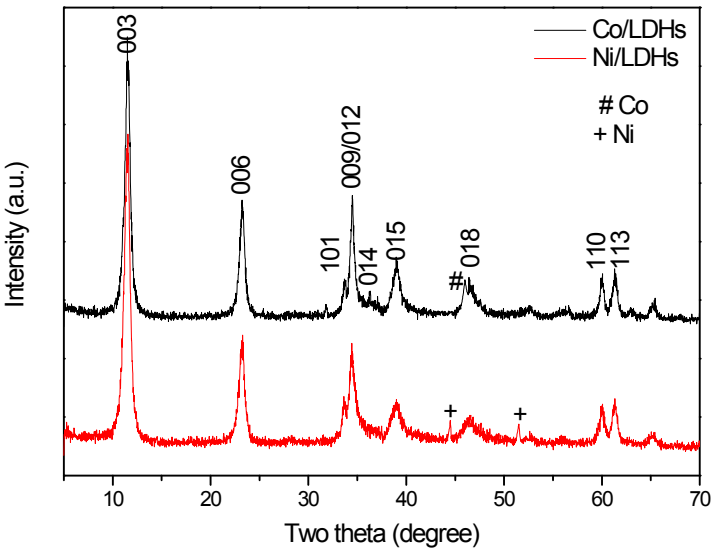

Figure S2 XRD curves for Co/LDHs and Ni/LDHs.

Table S1 Chemical composition of Au–Co,Ni alloy nanoparticles supported layered double hydroxides.

Sample	Chemical formula	Au (wt%)	Co/Ni (wt%)	Zn (wt%)	Al (wt%)	Au/Co or Au/Ni (mol%)
1	$Zn_{0.75}Al_{0.25}(OH)_2$ $(CO_3^{2-})_{0.13}$ $0.50H_2O$	–	–	45.8	6.34	–
2	$Au_{0.025}/Zn_{0.76}Al_{0.24}(OH)_2$ $(CO_3^{2-})_{0.12}$ $0.53H_2O$	4.39	–	44.4	5.80	–
3	$Co_{0.03}/Zn_{0.76}Al_{0.24}(OH)_2$ $(CO_3^{2-})_{0.12}$ $0.52H_2O$	–	1.63	45.7	5.98	–
4	$Ni_{0.03}/Zn_{0.76}Al_{0.24}(OH)_2$ $(CO_3^{2-})_{0.12}$ $0.55H_2O$	–	1.62	45.6	5.95	–
5	$Au_{0.0224}Co_{0.0026}/Zn_{0.75}Al_{0.25}(OH)_2$ $(CO_3^{2-})_{0.13}$ $0.48H_2O$	3.95	0.15	44.1	6.12	$9{:}1^{*}(8.62{:}1)^{\#}$
6	$Au_{0.0195}Co_{0.0055}/Zn_{0.75}Al_{0.25}(OH)_2$ $(CO_3^{2-})_{0.13}$ $0.49H_2O$	3.47	0.29	44.3	6.13	$4{:}1^{*}(3.55{:}1)^{\#}$
7	$Au_{0.0170}Co_{0.0080}/Zn_{0.76}Al_{0.24}(OH)_2$ $(CO_3^{2-})_{0.12}$ $0.52H_2O$	3.04	0.43	44.9	5.88	$2.33{:}1^{*}(2.13{:}1)^{\#}$
8	$Au_{0.0141}Co_{0.0109}/Zn_{0.76}Al_{0.24}(OH)_2$ $(CO_3^{2-})_{0.12}$ $0.50H_2O$	2.53	0.59	45.2	5.91	$1.5{:}1^{*}(1.29{:}1)^{\#}$
9	$Au_{0.0121}Co_{0.0129}/Zn_{0.76}Al_{0.24}(OH)_2$ $(CO_3^{2-})_{0.12}$ $0.50H_2O$	2.18	0.69	45.2	5.93	$1{:}1^{*}(0.94{:}1)^{\#}$
10	$Au_{0.0222}Ni_{0.0028}/Zn_{0.75}Al_{0.25}(OH)_2$ $(CO_3^{2-})_{0.13}$ $0.46H_2O$	3.98	0.15	44.3	6.13	$9{:}1^{*}(8.26{:}1)^{\#}$
11	$Au_{0.0192}Ni_{0.0058}/Zn_{0.76}Al_{0.24}(OH)_2$ $(CO_3^{2-})_{0.12}$ $0.51H_2O$	3.42	0.31	44.8	5.87	$4{:}1^{*}(3.31{:}1)^{\#}$
12	$Au_{0.0171}Ni_{0.0079}/Zn_{0.76}Al_{0.24}(OH)_2$ $(CO_3^{2-})_{0.12}$ $0.53H_2O$	3.05	0.42	44.8	5.86	$2.33{:}1^{*}(2.17{:}1)^{\#}$
13	$Au_{0.0138}Ni_{0.0112}/Zn_{0.75}Al_{0.25}(OH)_2$ $(CO_3^{2-})_{0.13}$ $0.50H_2O$	2.47	0.60	44.5	6.16	$1.5{:}1^{*}(1.24{:}1)^{\#}$
14	$Au_{0.0121}Ni_{0.0129}/Zn_{0.76}Al_{0.24}(OH)_2$ $(CO_3^{2-})_{0.12}$ $0.55H_2O$	2.18	0.68	44.9	5.89	$1{:}1^{*}(0.96{:}1)^{\#}$

Note: The content of Au, Co, Ni, Zn and Al elements are tested by ICP–AES, content of C, H and N is obtained from elementary analysis. * and # mean the theoretical and exact mole ratio of Au/Co or Au/Ni in samples, respectively.

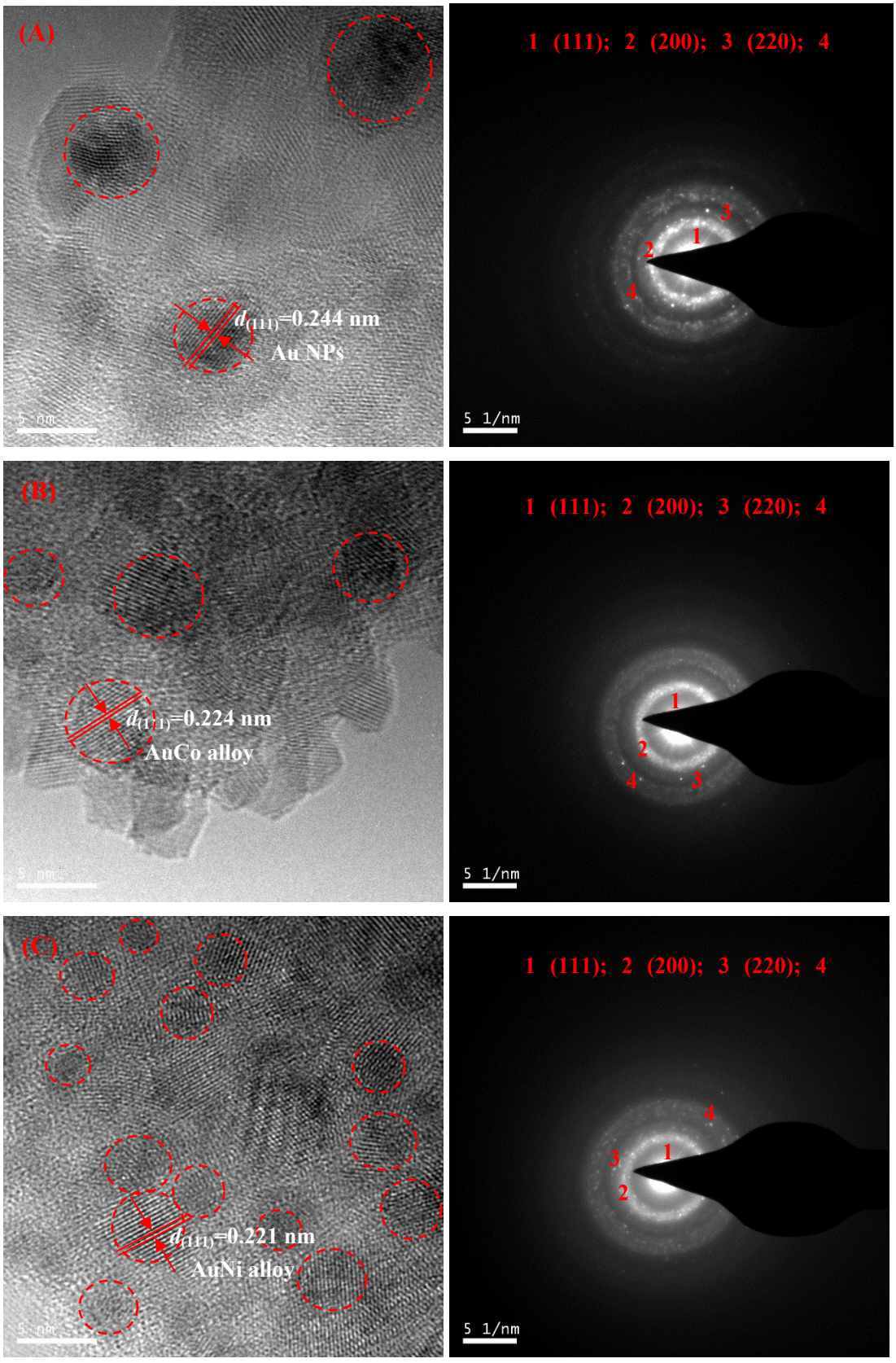

Figure S3 HRTEM image and Electron diffraction pattern (SAED) of Au–Co/LDHs (A) and Au–Ni/LDHs (B).

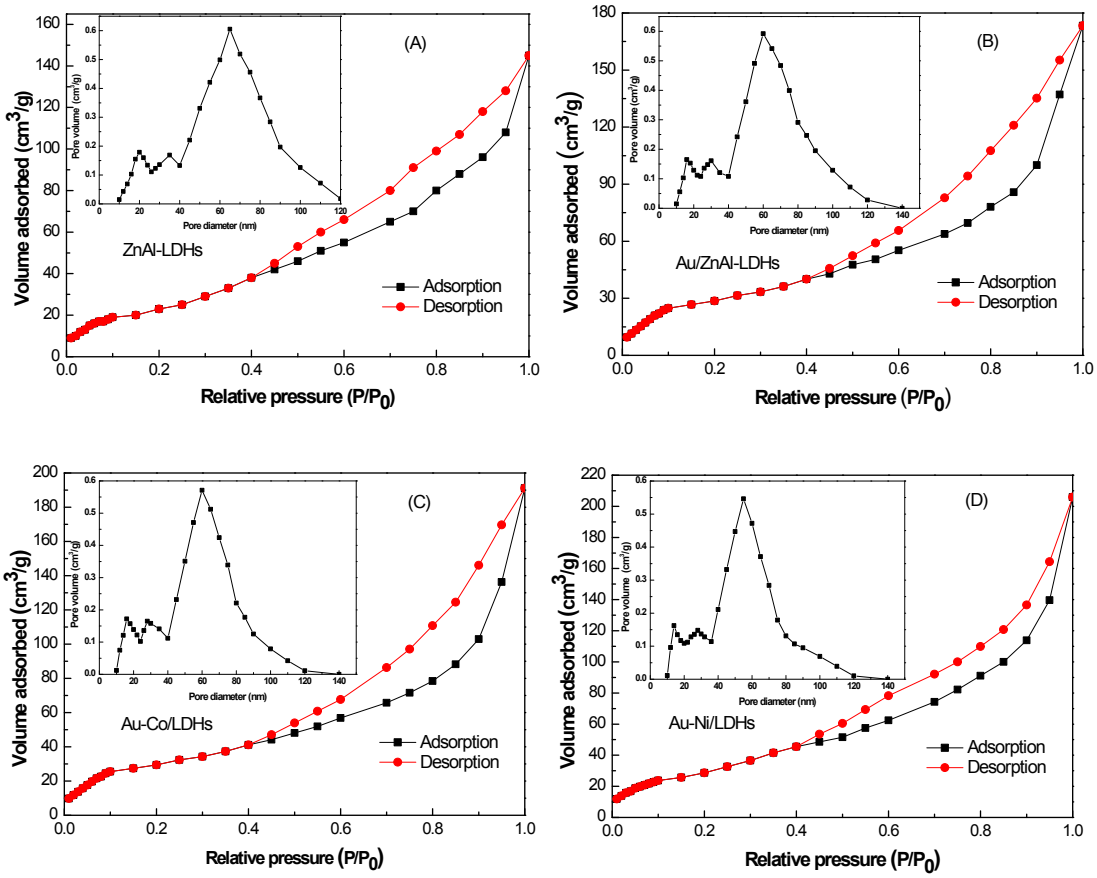

Figure S4 Pore size distribution and N_2 sorption isotherms for ZnAl–LDHs, Au/LDHs, Au–Co/LDHs (sample 6) and Au–Ni/LDHs (sample 11).

Table S2 The textural properties of ZnAl–LDHs, Au/LDHs, Au–Co/LDHs (sample 6) and Au–Ni/LDHs (sample 11).

Sample	Surface area (m^2/g)	Pore size distribution (nm)
ZnAl–LDHs	92.3	16, 30, 65
Au/LDHs	105.4	16, 30, 60
Au_4Co_1/LDHs	119.6	16, 28, 60
Au_4Ni_1/LDHs	128.9	14, 28, 55

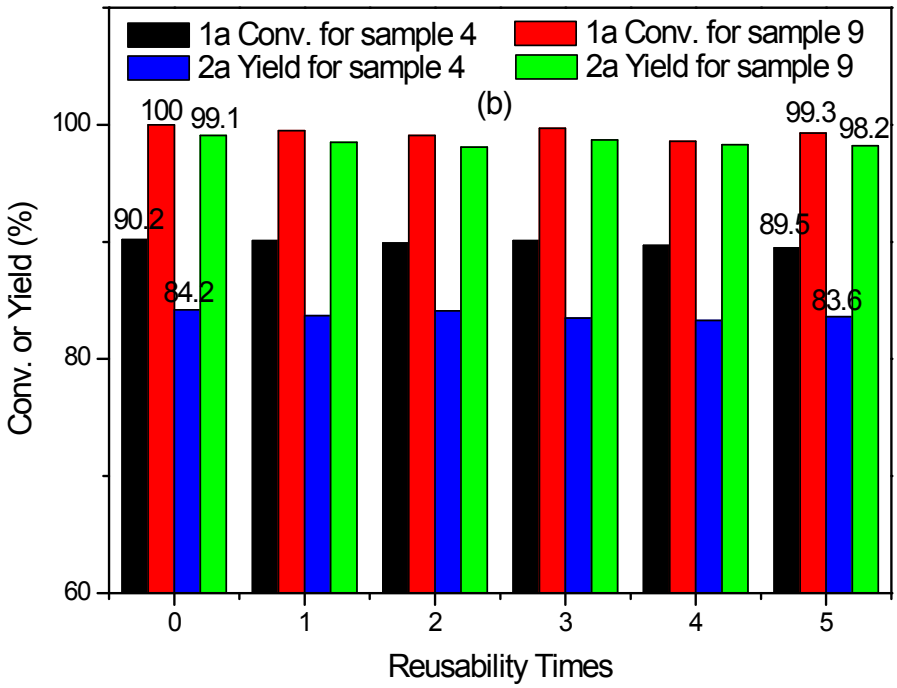

Figure S5 Reusability contrast of selective hydrogenation of crotonaldehyde to crotonyl alcohol over different samples.

2.2 Selective hydrogenation supplements

Table S3 Summary of reaction conditions and catalytic activities of selective hydrogenation of CDE to COL over various supported catalysts.

Entry	Catalyst	T/°C	P_{H2}/MPa	Conv.	Select.	TOF/h^{-1}	Reference
1	Ir/MgO, $Fe(NO_3)_3$	30	8	99	99	86	ACS Catal. 2017, 7, 5103
2	Ir–NbO_x/SiO_2	100	0.1	41.6	92.8	0.21 s^{-1}	ACS Sustainable Chem. Eng. 2017, 5, 3685
3	Fe/Pt/ ($La_2O_2CO_3$)	70	2.0	92.2	33.6	11.3	Reac. Kinet. Mech. Cat. 2017, 122, 117
4	γ–Mo_2N	70	1.0	94	27	–	ACS Catal. 2016, 6, 5797
5	Ir–MoO_x/SiO_2	30	0.8	78.9	94.2	125	ACS Catal. 2016, 6, 3600
6	3Ir/0.1Fe/SiO_2	50	0.1	65.6	90.8	64.8	J. Phys. Chem. C 2016, 120, 8663
7	Ir/Mo_2C	100	2.0	99	80	165	Chem. Eur. J. 2016, 22, 5698
8	Pt/$La(OH)_3$–700–NR	70	2.0	93.8	27.6	–	J. Nanopart. Res. 2016, 18, 66
9	Au@ZIF–8	80	0.5	9–80	50–95	–	ChemCatChem 2016, 8, 855
10	Ir–(Cr–Fe)/SiO_2	50	0.1	23–74.9	81.8–87.1	21.6–61.8	Catal. Sci. Technol. 2016, 6, 4294
11	Au,Ag/SBA–15	120	3.0	98.7–99.9	43.2–58.8	48.4–183	J. Catal. 2015, 330, 135
12	Pt,Sn/TiO_2	80	0.1	<80	<60	90–200	Phys. Chem. Chem. Phys. 2015, 17, 28186
13	Pt_3Sn/SnO_2/rGO	70	2.0	99	90.1	–	Catal. Sci. Technol. 2015, 5, 3108
14	Ru–Ir/ZnO	80	0.1	27.5–93.5	80.8–94.6	<9	J. Mol. Catal. A–Chem. 2014, 392, 89
15	Pt/ZnO	80	0.1	10.6	95	7.2	Appl. Catal. B 2014, 154–155, 369
16	Ir/SiO_2	80	0.1	4.6–15.7	54.9–77.6	<17.3	Appl. Surf. Sci. 2013, 270, 388

17	Au/Mesoporous titania	200	–	<25	<82	–	Micropor. Mesopor. Mat. 2013, 168, 51
18	Ir–ReO*x*/SiO_2	30	0.8	99	91	–	Chem. Commun. 2013, 49, 7034
19	Cu/MCM–48	100	1.0	<80	<55	<7.2	Appl. Catal. A–Gen. 2012, 437– 438, 72
20	Au/C	60	0.2	34	37	54	ACS Catal. 2012, 2, 671
21	Sn/Pt/SiO_2	100	2.0	6	10	36.8	J. Catal. 2012, 288, 84
22	Ir/ZrO_2	80	0.1	<31.6	<82.2	<54.7	Catal. Commun. 2012, 21, 5
23	Ir/TiO_2	80	0.1	<26.9	<74.6	<13.7	Appl. Catal. A–Gen. 2012, 433–434, 236

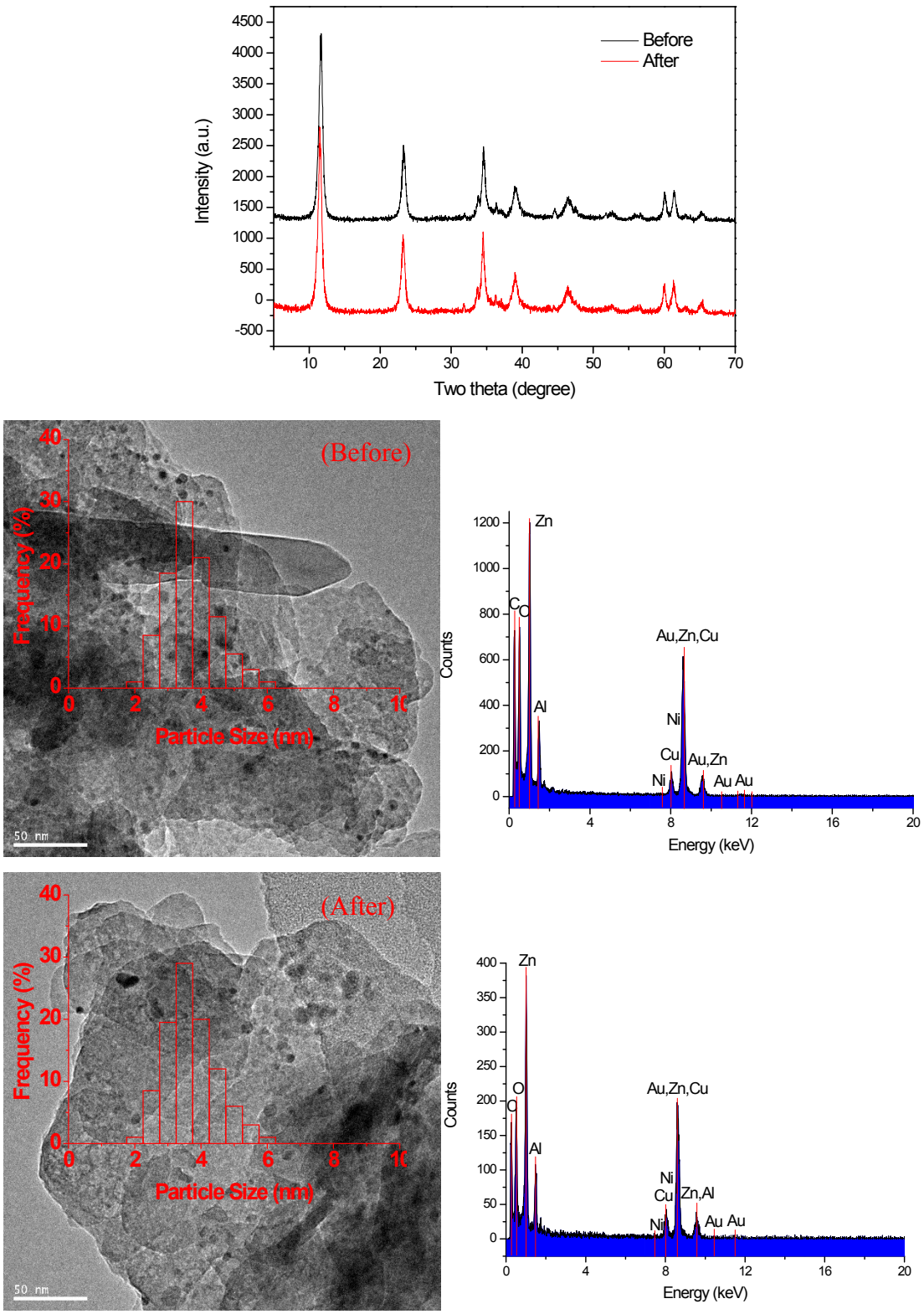

Figure S6 Comparison of XRD, TEM and EDX analysis of Au–Ni/LDHs (sample 9) before and after catalysis.

2.3. Adsorption of CDE (E_{ads}) at the surface of Au–Co,Ni/LDHs

2.3.1 Adsorption models and adsorption energy

CDE is adsorbed at the surface of Au–Co,Ni/LDHs first, and then it reacts with the dissociated H atoms for the hydrogenation reaction, finally, the product moves out of the catalyst surface and finish the reaction. Therefore, the adsorption step is the key point to study CDE hydrogenation. Based on the references, CDE has both single point (O, C=O and C–C) and double points (O cooperate with C=C or C=O cooperate with C=C) adsorption. CDE could be single adsorbed at Au–Co/LDHs on the following seven spots: Top_{Au}, Top_{Co}, $Bri_{Au–Au}$, $Bri_{Au–Co}$, $Bri_{Co–Co}$, Hcp and Fcc. There are 21 models for single point adsorption and 49 for double points adsorption. In this paper we totally optimized 70 models of them. At the surface of Au–Ni/LDHs, CDE could single adsorbed at Top_{Au}, Top_{Ni}, $Bri_{Au–Au}$, $Bri_{Au–Ni}$, Hcp and Fcc. There are totally 18 single point adsorptions and 36 double points adsorptions, we calculated all 54 of them in this paper as well. To quantitatively compare adsorption, we introduced the concept of adsorption energy (E_{ads}). The definition equation is $E_{ads}=E_{CDE}+E_{Au–Co,Ni/LDHs}–E_{CDE/Au–Co,Ni/LDHs}$, in which $E_{CDE/Au–Co,Ni/LDHs}$ means the energy of system when CDE is absorped on Au–Co,Ni/LDHs. The higher of the E_{ads} value means the more stable of the system.

Table S4 and **S5** list the optimized CDE adsorption models, their E_{ads} values and the height of O atm distanced from surface ($d_{O–layer}$). There are only 22 and 17 stable adsorption models at the surface of Au–Co/LDHs and Au–Ni/LDHs, respectively.

The decrease of adsorption models could be caused by the adsorption energy increase due to the modified element at the surface of Au–Co,Ni/LDHs.

Table S4 Calculation result of CDE adsorption on different sites of Au–Co/LDHs surface.

FNial adsorption mode	E_{ads} /(kJ·mol^{-1})	$d_{O-layer}$ /nm	FNial adsorption mode	E_{ads} /(kJ·mol^{-1})	$d_{O-layer}$ /nm
η_1–O(Top_{Au})	89.99	0.310	η_4–πCO(Top_{Au})–πCC(Top_{Co})	91.68	0.325
η_1–O(Top_{Co})	124.09	0.173	η_4–πCO(Top_{Co})–πCC(Top_{Co})	93.25	0.313
η_1–O(Bri_{Au-Au})	88.68	0.313	η_4–πCO(Bri_{Au-Co})–diσCC(Top_{Co})	96.20	0.301
η_2–πCO(Top_{Au})	93.39	0.313	η_4–πCO(Top_{Co})–diσCC(Bri_{Au-Co})	105.34	0.306
η_2–diσCO(Top_{Co})	152.21	0.233	η_4–diσCO(Top_{Au})–πCC(Hcp)	92.01	0.314
η_2–diσCO(Bri_{Au-Co})	116.33	0.293	η_4–diσCO(Bri_{Au-Au})–πCC(Top_{Co})	92.96	0.315
η_2–diσCO(Bri_{Co-Co})	87.67	0.328	η_4–diσCO(Bri_{Au-Co})–πCC(Bri_{Co-Co})	94.51	0.315
η_2–πCC(Top_{Co})	88.29	0.458	η_4–diσCO(Hcp)–πCC(Top_{Co})	94.99	0.306
η_2–diσCC(Bri_{Au-Co})	88.79	0.449	η_4–diσCO(Bri_{Au-Co}) –diσCC(Bri_{Au-Au})	89.79	0.333
η_2–diσCC(Bri_{Co-Co})	93.66	0.381	η_4–diσCO(Fcc)–diσCC(Fcc)	90.90	0.311
η_3–diσCC(Top_{Au}) –σO(Bri_{Au-Au})	89.67	0.321			
η_3–diσCC(Top_{Au}) –σO(Hcp)	89.98	0.331			

At the same time, the uneven electron distribution at Au–Co,Ni/LDHs may also contribute to this decrease. Particularly, the double points adsorption decreased down to 9 and 12, which could be caused by the fact that steric hindrance of CH_3 is stronger than the C=C adsorption. The adsorption energy is 79.88–145.45 kJ/mol for CDE/Au–Ni/LDHs system, the distance between oxygen and the catalyst surface is 0.242–0.595 nm. When CDE is adsorbed at Top_{Ni} (η_2–diσCO(Top_{Ni})), it has the highest adsorption energy of 145.45 kJ/mol, the oxygen is 0.242 nm to the catalyst surface. The C=O and C=C bonds are stretched to 0.003 and 0.002 nm, and the C–C

connecting C=O and C=C decreased about 0.02, it shows that this adsorption makes the bond length even. The adsorption energy and the $d_{O–layer}$ values are 85.18–152.21 kJ/mol and 0.173–0.471 nm for CDE/Au–Co/LDHs system. When CDE is adsorbed on $Top_{Co}(\eta_2–di\sigma CO(Top_{Co}))$, the adsorption energy peaks with a value of 152.21 kJ/mol, at the same time the $d_{O–layer}$ is 0.233 nm. The C=O and C=C bond lengths are increased by 0.004 nm and 0.002 nm, the C–C between C=O and C=C decreased by 0.003 nm. This type of adsorption also evens out the bond lengths. **Figure S7** are the most stable adsorption models of CDE at Au–Co/LDHs and Au–Ni/LDHs.

Table S5 Calculation result of CDE adsorption at different sites of Au–Ni/LDHs surface.

Final adsorption mode	E_{ads} /(kJ·mol^{-1})	$d_{O–layer}$ /nm	Final adsorption mode	E_{ads} /(kJ·mol^{-1})	$d_{O–layer}$ /nm
$\eta_1–O(Top_{Ni})$	135.66	0.244	$\eta_4–\pi CO(Top_{Au})–\pi CC(Top_{Ni})$	85.00	0.333
$\eta_1–O(Bri_{Au–Au})$	89.65	0.253	$\eta_4–\pi CO(Bri_{Au–Ni})–\pi CC(Top_{Au})$	85.12	0.335
$\eta_2–di\sigma CO(Top_{Ni})$	145.45	0.242	$\eta_4–\pi CO(Bri_{Au–Au})–\pi CC(Top_{Ni})$	86.27	0.327
$\eta_2–di\sigma CO(Bri_{Au–Au})$	85.37	0.346	$\eta_4–\pi CO(Top_{Au})–di\sigma CC(Bri_{Au–Ni})$	86.96	0.320
$\eta_2–\pi CC(Top_{Au})$	79.88	0.595	$\eta_4–\pi CO(Top_{Ni})–di\sigma CC(Fcc)$	84.32	0.335
$\eta_2–\pi CC(Top_{Ni})$	83.06	0.470	$\eta_4–di\sigma CO(Fcc)–\pi CC(Bri_{Au–Ni})$	83.03	0.338
$\eta_2–di\sigma CC(Bri_{Au–Au})$	85.50	0.453	$\eta_4–di\sigma CO(Hcp)–di\sigma CC(Top_{Au})$	83.98	0.334
$\eta_2–di\sigma CC(Hcp)$	87.20	0.441	$\eta_4–di\sigma CO(Fcc)–di\sigma CC(Hcp)$	83.28	0.335
$\eta_3–di\sigma CC(Fcc)–\sigma O(Top_{Au})$	82.90	0.329			

E_{ads} represents the adsorption energies; $d_{O–layer}$ represents the distance between O atom and layer.

In a conclusion, the most stable adsorption for CDE at Au–Co/LDHs and Au–Ni/LDHs surfaces is the σ bonded chemical adsorption at Top_M (the largest adsorption

energy). CDE has slightly higher adsorption energy at the surface of Au–Co/LDHs compared to Au–Ni/LDHs, which are both higher than the unmodified Au/LDHs (93.70 kJ/mol). In addition, the C=O bond length of CDE is changed more dramatically at Au–Co/LDHs compared to Au–Ni/LDHs, which may make C=O easier to break. To summarize, Au–Co/LDHs surface has higher adsorption for CDE than Au–Ni/LDHs which can activate C=O better.

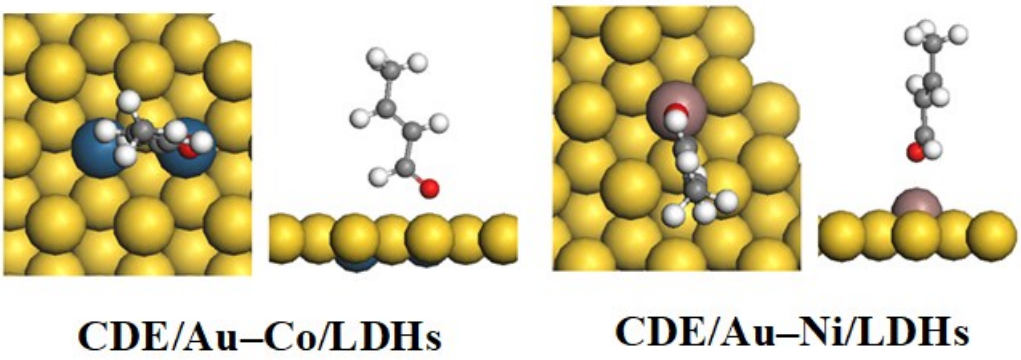

Figure S7 The most stable adsorption configurations of CDE on Au–Co,Ni/LDHs surfaces.

2.3.2 Electronic properties analysis of adsorption models

To further understand the electron interaction between CDE and Au–Co,Ni/LDHs, we calculated the densities of states of the most stable model as **Figure S8** shows. For CDE/Au–Co,Ni/LDHs, the electron hybrid between CDE and Au–Co,Ni/LDHs surface is weak at the range of –17.18 eV to –7.04 eV, but the *s* and *p* orbital hybrid inside CDE molecule is strong and therefore we can assume the covalent bonding is dominating. At around –7.04 eV to Fermi level, the *d* orbital of Au–Co,Ni/LDHs is hybriding with *p* orbital of CDE, which contributes to the CDE adsorption at Au–

Co,Ni/LDHs. The hybrid between the *d* orbital of Au–Co,Ni/LDHs and the *s* orbital of CDE also helps. The Dirac function diagrams between these two systems are similar which tells that the adsorption and bonding is the same, this is also consistent with our surface adsorption results.

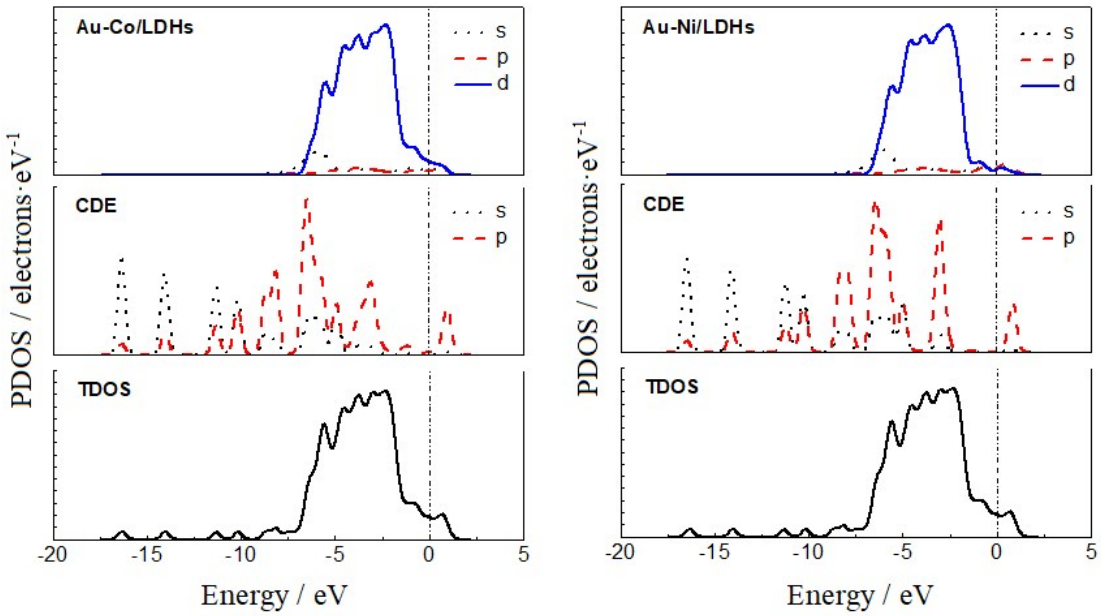

Figure S8 Densities of states of CDE adsorption on Au–Co,Ni/LDHs surfaces.

Note: the dash dot represents the Fermi level.

Deformation charge density (DCD) graph can describe the electron rearrangement after adsorption and help understanding the electron interaction between CDE and Au–Co,Ni/LDHs. We calculated the DCD for the most stable adsorption model in this paper. As **Figure S9** shows, the DCD is defined by the formula: $\Delta\rho=\rho_{CDE/Au–Co,Ni/LDHs}-\rho_{CDE}-\rho_{Au–Co,Ni/LDHs}$, in which $\rho_{CDE/Au–Co,Ni/LDHs}$, ρ_{CDE} and $\rho_{Au–Co,Ni/LDHs}$ represent the total charge density, charge density of CDE and charge density of Au–Co,Ni/LDHs, respectively. The blue region in the graph represents the lost electrons,

and red region is the gained electrons, the deeper of the color and the larger of the colored area represent the larger number of gained or lost electrons. From **Figure S9**, CDE has similar patterns at the Au–Co,Ni/LDHs, which further supports our conclusion that CDE has the same adsorption at both Au–Co/LDHs and Au–Ni/LDHs. At the same time, CDE/Au–Co/LDHs system has deeper and larger colored area compared to CDE/Au–Ni/LDHs, which means Au–Co/LDHs has stronger adsorption for CDE than Au–Ni/LDHs, this conclusion again supports our results of adsorption energy analysis.

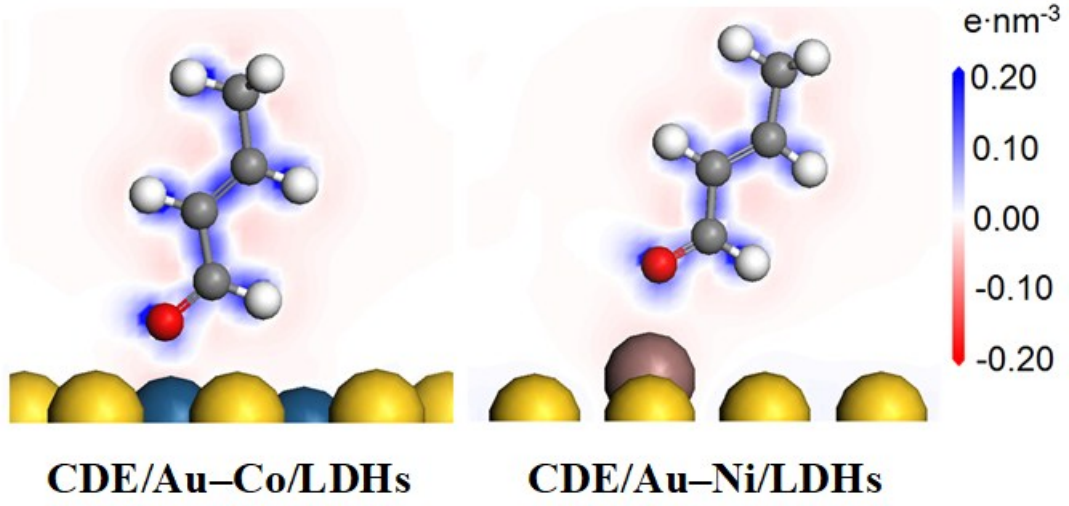

Figure S9 Deformation density of CDE adsorption on Au–Co,Ni/LDHs surfaces. Note: the blue and red represent the region which electron density is decreased and increased after adsorption, respectively.

2.4 Hydrogenation mechanism analysis supplements

Table S6 Adsorption energies and distance of CDE hydrogenation products on Au–Co,Ni/LDHs surface

Surface	E_{ads}/eV				*d*/nm			
	COL	ENOL	BDE	BOL	COL	ENOL	BDE	BOL
Au–Co/LDHs	1.334	1.249	1.043	0.995	0.245	0.254	0.280	0.295
Au–Ni/LDHs	1.361	1.250	1.031	0.976	0.243	0.254	0.283	0.299

Table S7 Different reaction mechanisms for the partial hydrogenation of CDE

Step	Mechanism A	Mechanism B	Mechanism C
1	CDE+*→CDE*	CDE+*→CDE*	CDE+*→CDE*
2	H_2+*→H_2*	H_2+*→H_2*	H_2+*→H_2*
3	H_2*→H*+H*	H_2*→H*+H*	H2*→H*+H*
4	CDE*+H*→MS2*(A1) Or CDE*+H*→MS1*(A2)	CDE*+H*→MS4*(B1) Or CDE*+H*→MS3*(B2)	CDE*+H*→MS2*(C1) Or CDE*+H*→MS3*(C2)
5	MS2*+H*→COL*(A1) Or MS1*+H*→COL*(A2)	MS4*+H*→BDE*(B1) Or MS3*+H*→BDE*(B2)	MS2*+H*→ENOL*(C1) Or MS3*+H*→ENOL*(C2)
6	COL*→COL+*	BDE*→BDE+*	ENOL*→ENOL+*
General reaction	CDE+H_2→COL	CDE+H_2→BDE	CDE+H_2→ENOL

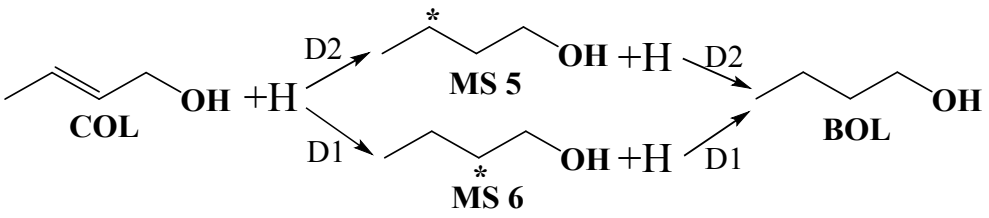

Figure S10 Different reaction mechanisms for the selective hydrogenation of COL.

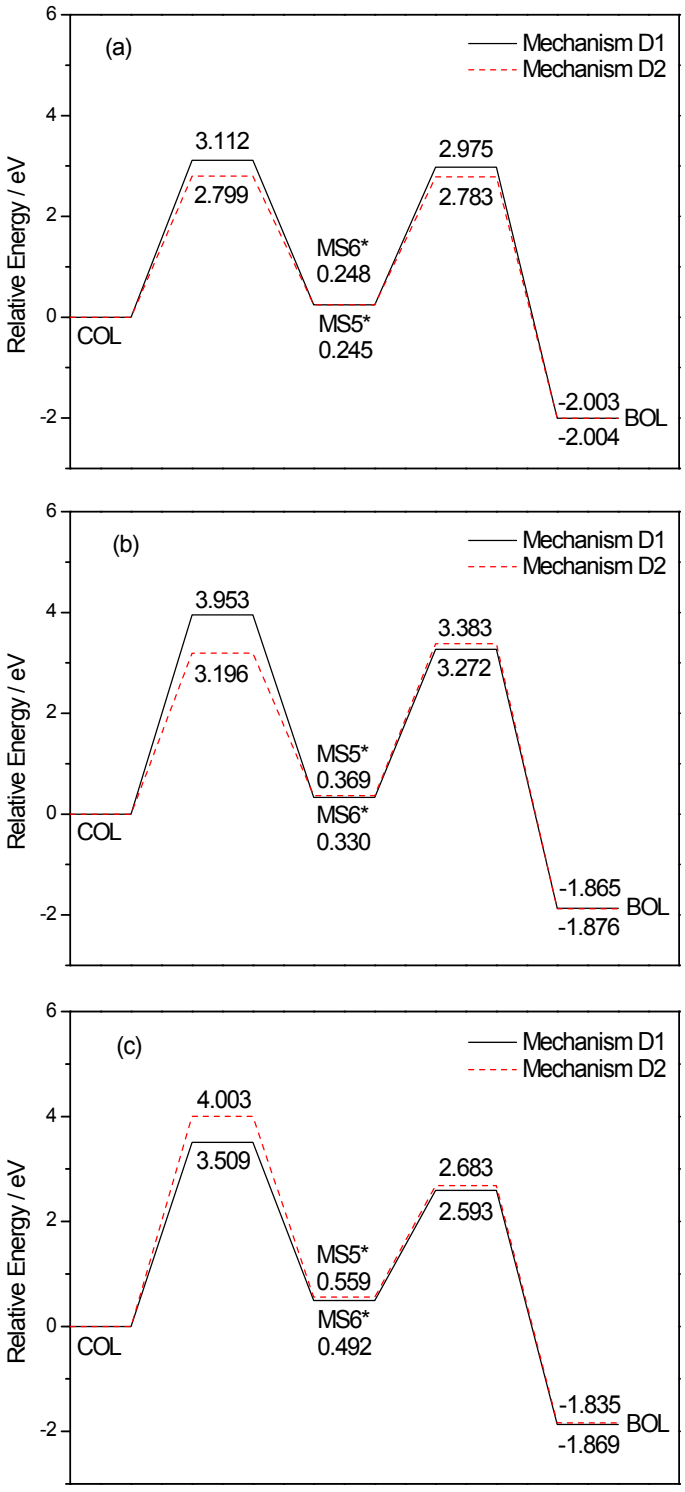

Figure S11 Schematic diagram for potential relative energy of reaction mechanisms for COL on Au/LDHs (a), Au–Co/LDHs (b) and Au–Ni/LDHs surface (c).

2.5. Spectral data for main products

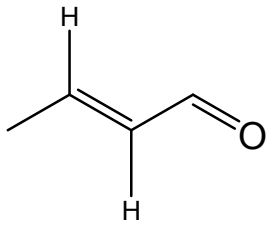

(CAS NO: 4170–30–3)

Crotonaldehyde (1a): ^{1}H NMR (500 MHz, $CDCl_3$, TMS): δ 2.04 (s, 3H), 6.03 (s, 1H), 6.61 (s, 3H), 9.62 (m, 1H). ^{13}C NMR (125 MHz, $CDCl_3$, TMS): δ 18.5, 133.6, 153.5, 192.9.

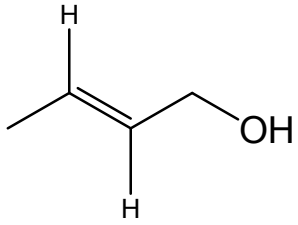

(CAS NO: 6117–91–5)

crotonyl alcohol (2a): ^{1}H NMR (500 MHz, $CDCl_3$, TMS): δ 2.02 (m, 3H), 3.61 (s, 1H), 4.13 (m, 2H), 5.63–5.67 (m, 1H). ^{13}C NMR (125 MHz, $CDCl_3$, TMS): δ 17.1, 63.5, 125.6, 130.2.

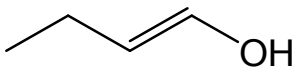

The structure of enol (3a) is instable.

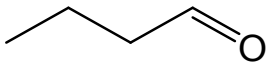

(CAS NO: 123–72–8)

butyraldehyde (4a): ^{1}H NMR (500 MHz, $CDCl_3$, TMS): δ 0.88 (m, 3H), 1.70 (m, 2H), 2.36 (m, 2H), 9.67 (s, 1H). ^{13}C NMR (125 MHz, $CDCl_3$, TMS): δ 13.2, 15.1, 45.4, 201.9.

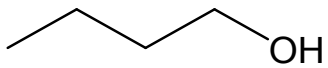

(CAS NO: 71–36–3)

butanol (5a): ^{1}H NMR (500 MHz, $CDCl_3$, TMS): δ 0.89 (m, 3H), 1.43 (m, 2H), 1.51 (m, 2H), 3.47 (m, 2H), 3.62 (s, 1H). ^{13}C NMR (125 MHz, $CDCl_3$, TMS): δ 13.9, 18.4, 34.1, 62.2.